Article

Cell Reports

Intratumoral Myeloid Cells Regulate Responsiveness and Resistance to Antiangiogenic Therapy

Graphical Abstract

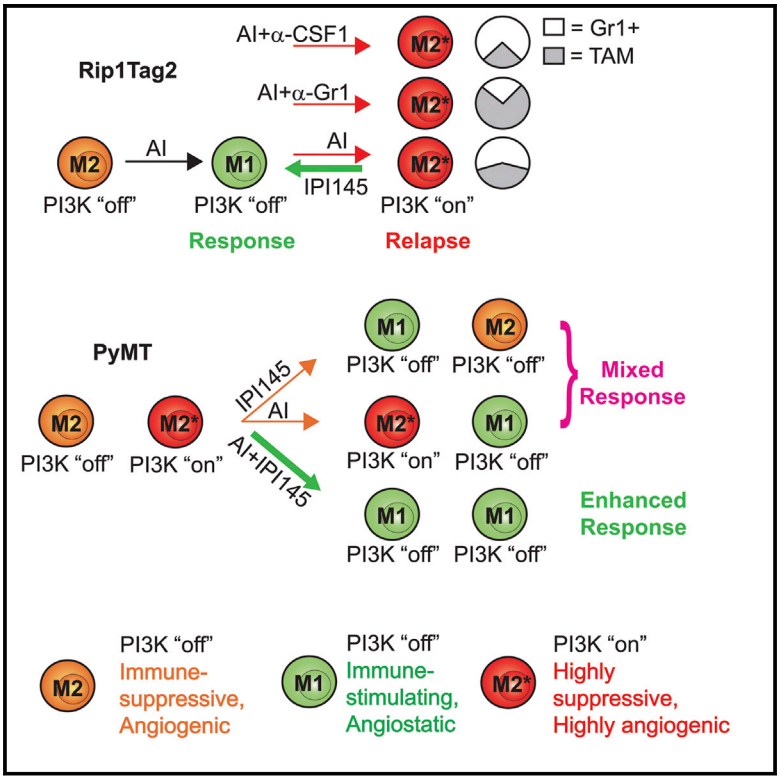

Authors

Lee B. Rivera, David Meyronet, ..., Emily Bergsland, Gabriele Bergers

Correspondence

gabriele.bergers@ucsf.edu

In Brief

Antiangiogenic therapy typically results in transient tumor response. Rivera et al. show that therapy induces antitumor behavior in myeloid cells, which subsequently become tumor promoting via PI3K activation. Targeting distinct myeloid populations results in increases in nontargeted myeloid cells, creating an oscillating pattern of resistance. Myeloid-cell PI3K inhibition overcomes such resistance and enhances therapeutic efficacy.

Highlights

- Sensitivity to VEGF/VEGFR inhibition is driven by myeloid-cell-derived CXCL14
- Myeloid PI3K activation overrides sensitivity and promotes angiogenic relapse
- Myeloid-cell oscillation in tumors maintains resistance to antiangiogenic therapy
- Inhibition of myeloid PI3K activity overcomes resistance to antiangiogenic therapy

Rivera et al., 2015, Cell Reports *11*, 577–591
April 28, 2015
http://dx.doi.org/10.1016/j.celrep.2015.03.055

CellPress

Cell Reports
Article

Intratumoral Myeloid Cells Regulate Responsiveness and Resistance to Antiangiogenic Therapy

Lee B. Rivera,[1] David Meyronet,[2] Valérie Hervieu,[3] Mitchell J. Frederick,[4] Emily Bergsland,[5] and Gabriele Bergers[1,*]
[1]Department of Neurological Surgery, Brain Tumor Research Center, Helen Diller Family Comprehensive Cancer Center, University of California, San Francisco, San Francisco, CA 94158, USA
[2]Université Lyon 1, Centre de Pathologie et Neuropathologie Est, Hospices Civils de Lyon, Bron Cedex 69677, France
[3]Université Lyon 1, Service d'Anatomie Pathologique, Hôpital Édouard Herriot, Hospices Civils de Lyon, Lyon Cedex 69003, France
[4]Department of Head and Neck Surgery, Research Division of Surgery, The University of Texas MD Anderson Cancer Center, Houston, TX 77030, USA
[5]Department of Medicine, UCSF Mount Zion Cancer Center, University of California, San Francisco, San Francisco, CA 94143, USA
*Correspondence: gabriele.bergers@ucsf.edu
http://dx.doi.org/10.1016/j.celrep.2015.03.055

SUMMARY

Antiangiogenic therapy is commonly used in the clinic, but its beneficial effects are short-lived, leading to tumor relapse within months. Here, we found that the efficacy of angiogenic inhibitors targeting the VEGF/VEGFR pathway was dependent on induction of the angiostatic and immune-stimulatory chemokine CXCL14 in mouse models of pancreatic neuroendocrine and mammary tumors. In response, tumors reinitiated angiogenesis and immune suppression by activating PI3K signaling in all CD11b+ cells, rendering tumors nonresponsive to VEGF/VEGFR inhibition. Adaptive resistance was also associated with an increase in Gr1+CD11b+ cells, but targeting Gr1+ cells was not sufficient to further sensitize angiogenic blockade because tumor-associated macrophages (TAMs) would compensate for the lack of such cells and vice versa, leading to an oscillating pattern of distinct immune-cell populations. However, PI3K inhibition in CD11b+ myeloid cells generated an enduring angiostatic and immune-stimulatory environment in which antiangiogenic therapy remained efficient.

INTRODUCTION

Antiangiogenic therapy represents one of the most widely used anticancer strategies today, with most approved therapies targeting the vascular endothelial growth factor (VEGF) signaling pathway. However, since the beneficial effects observed across the multitude of cancers that respond to such treatment are typically short-lived, much effort has focused on uncovering the various mechanisms whereby tumors bypass the tumor-inhibitory effects of therapy (Bergers and Hanahan, 2008; Kerbel, 2008). One such resistance mechanism involves reinstatement of angiogenesis by tumor-infiltrating innate immune cells (De Palma et al., 2005; Fischer et al., 2007; Shojaei et al., 2007a, 2007b).

Tumors can contain a significant percentage of different infiltrating myeloid cells with bivalent functions, but predominantly are thought to support tumor progression by promoting angiogenesis and suppressing antitumor immunity. Tumor-associated macrophages (TAMs) are typically characterized as either "classically" activated tumoricidal macrophages (M1) or "alternatively" activated protumorigenic macrophages (M2) (Mantovani et al., 2008). Extending this nomenclature, tumor-associated neutrophils (TANs) have also been categorized as N1 or N2 based on their anti- or protumor activity in tumors (Fridlender et al., 2009). In addition, immature Gr1+ cells with either a mononuclear or granular morphology have been identified in tumors that convey immune-suppressive functions, and thus are also termed myeloid-derived suppressor cells (M-MDSC and G-MDSC, respectively) (Talmadge and Gabrilovich, 2013). Typically, surface-marker profiling based on expression of CD11b, F4/80, Gr1, Ly6C, and Ly6G is used to categorize these subsets of tumor-infiltrating myeloid cells (Fridlender et al., 2009; Talmadge and Gabrilovich, 2013; Wynn et al., 2013).

There is mounting evidence that tumors recruit these distinct populations, which then become an additional source of angiogenic chemokines and cytokines to promote angiogenesis (Coussens et al., 2000; Du et al., 2008; Giraudo et al., 2004; Lin et al., 2006; Shojaei et al., 2007b). Given that hypoxia is a major driver of myeloid-cell recruitment (Du et al., 2008; Mazzieri et al., 2011), it is conceivable that therapy-induced hypoxia via an angiogenic blockade can induce factors that mobilize cells from the bone marrow and attract them to the tumor site. Indeed, tumor-associated myeloid cells have been shown to sustain angiogenesis in the face of antiangiogenic therapy, in part by stimulating VEGF-independent pathways. For example, macrophages were shown to induce the expression of various angiogenic molecules, including *FGF-1*,*2*, *MMP9*, and *Ang2*, in response to antiangiogenic therapy (Casanovas et al., 2005; Fischer et al., 2007; Rigamonti et al., 2014), and Gr1+ myeloid

cells were found to convey resistance to anti-VEGF treatment via secretion of the angiogenic PKR-1/2 ligand Bv8 (Shojaei et al., 2007a, 2007b). Even though inhibitors of macrophages or Gr1+ cells enhanced the effects of antiangiogenic therapy, in many of these models tumor growth still occurred, albeit at a slower pace, throughout the duration of treatment. Here, we investigated the overall contributions of different tumor-associated myeloid populations to evasion of antiangiogenic therapy. We analyzed the composition and function of TAMs, TANs, and two Gr1+ immature monocyte populations in two distinct tumor models that responded differently to angiogenic inhibition. In the Rip1Tag2 model of pancreatic neuroendocrine tumor (PNET), angiogenic blockade was able to transiently reduce vessel density and block tumor growth (response) followed by reinstatement of neovascularization and robust tumor growth (relapse), which enabled us to evaluate true "response" and "relapse" phases in a single model. In the PyMT mammary carcinoma model, angiogenic blockade was only able to slow down tumor growth, with some reduction in vessel density, a feature that is commonly observed in various tumor models. Analysis of myeloid-cell content within tumors revealed that the angiogenic relapse was associated with an increase in tumor-specific subsets of Gr1+ myeloid cells. By investigating the role of these cells during relapse, we were able to uncover a compensatory nature of myeloid-cell-mediated resistance to antiangiogenic therapy. We sought to determine the mechanisms by which distinct innate immune cells compensate for each other to maintain resistance, and to identify ways to modulate inflammation so as to sustain the effects of antiangiogenic therapy.

RESULTS

Targeting Distinct Myeloid Subtypes Leads to a Compensatory Oscillation between Innate Immune Cells, Enabling Reneovascularization during Antiangiogenic Therapy

We established a model of evasive resistance to antiangiogenic therapy in the Rip1Tag2 (RT2) model of PNET. Treatment of 13-week-old tumor-bearing mice with the broad-spectrum angiokinase inhibitor sorafenib induced a 2- to 3-week period of response characterized by tumor stasis followed by robust tumor growth and subsequent death (Figure 1A). The onset of sorafenib response and relapse is similar to that observed with DC101, a VEGFR2-neutralizing antibody, supporting the notion that sorafenib predominantly blocks the VEGF/VEGFR2 pathway in PNET (Casanovas et al., 2005; Rigamonti et al., 2014; G.B., unpublished data). Tumor analysis during the response phase (2-week treatment, 15 weeks of age) with sorafenib revealed a substantial reduction in vessel density and hemorrhage formation, whereas relapsing tumors (4-week treatment, 17 weeks of age) exhibited a vascular pattern similar to that of untreated tumors, with high vessel density and hemorrhage recurrence (Figure 1B). Thus, we defined "responding" tumors as those treated from 13 to 15 weeks of age (2 weeks), and "relapse" tumors as those treated from 13 to 17 weeks of age (4 weeks). Therefore, RT2-PNETs overcome vascular growth restrictions by gaining the capability to reinitiate neovascularization. When we investigated the intratumoral composition of innate immune cells, fluorescence-activated cell sorting (FACS) analysis of PNETs during the course of treatment revealed no substantial difference in the number or composition of myeloid cells during the response phase (Figures 1C, S1A, S1B, and S2A). However, a substantial increase in intratumoral Gr1+Ly6C^{Hi} monocytes (SSC^{Low}CD11b+Gr1^{Low}Ly6C^{High}Ly6-G^{Low}) accompanied the angiogenic relapse (Figures 1C, S1A, and S2A). As elevated levels of infiltrating Gr1+ myeloid cells were previously found to promote tumor resistance to anti-VEGF therapy (Shojaei et al., 2007a), we targeted relapse-associated Gr1+ cells 2 weeks after the start of antiangiogenic therapy, when the tumors were still responding to sorafenib (Figure 1D). Although it blocked the increased accumulation of Gr1+ cells within the tumor (Figures 1F, S1A, S1B, and S2B), this approach did not prolong responsiveness to sorafenib and led to a proangiogenic relapse similar to that observed with sorafenib alone (Figure 1E). Furthermore, reducing Gr1+ cell infiltration induced a compensatory increase in TAMs to potentially confer therapeutic resistance (Figures 1F, S1A, S1B, and S2B). Hence, we investigated whether TAM depletion with a CSF1-neutralizing antibody would be more beneficial for sustaining a sorafenib response. However, this approach was also unable to prolong the response to antiangiogenic therapy (Figures 1G and 1H), as it induced an increase in intratumoral Gr1+Ly6G^{Hi} and Gr1+Ly6C^{Hi} monocytes and TAN (Figures 1I, S1A, and S2C). Thus, Gr1+ cells compensate for TAM depletion and vice versa—a phenomenon that is reminiscent of an oscillating pattern of innate immune cells to convey therapeutic resistance to antiangiogenic therapy. These results imply that several myeloid-cell populations regulate reneovascularization and promote it in a compensatory manner.

Upregulation of Angiostatic Chemokines Is Associated with the Antiangiogenic Effects of Sorafenib in PNET

To elucidate how myeloid-cell oscillation promotes a proangiogenic relapse during sorafenib therapy, we compared the gene expression of several prominent angiogenic factors among naive, responding, and relapsing PNETs of RT2 mice treated with sorafenib alone or in combination with either anti-Gr1 or anti-CSF1. Interestingly, compared with naive tumors, response-phase tumors displayed enhanced levels of several prominent proangiogenic factors despite exhibiting substantial vessel reduction (Figures 2A, S3A, and S3B). They remained at similar levels in the relapse phase regardless of whether the mice received sorafenib alone or in combination with anti-Gr1 or anti-CSF1 treatment (Figures 2A, S3A, and S3B). In contrast, expression analysis of various angiostatic chemokines in tumors showed that *CXCL14* was dominantly upregulated in responding tumors, followed to a lesser extent by *CXCL4* (Figures 2A, S3C, and S3D). Both chemokines returned to base level upon tumor relapse with sorafenib alone or in combination with anti-Gr1 or anti-CSF1 treatment. Expression of the angiogenic factor BV8 and antiangiogenic molecules thrombospondin-1 and thrombospondin-2 did not change throughout the duration of treatment (data not shown). These results suggest that in PNETs, the angiogenic response and relapse during sorafenib treatment is not determined by upregulation of proangiogenic factors, but

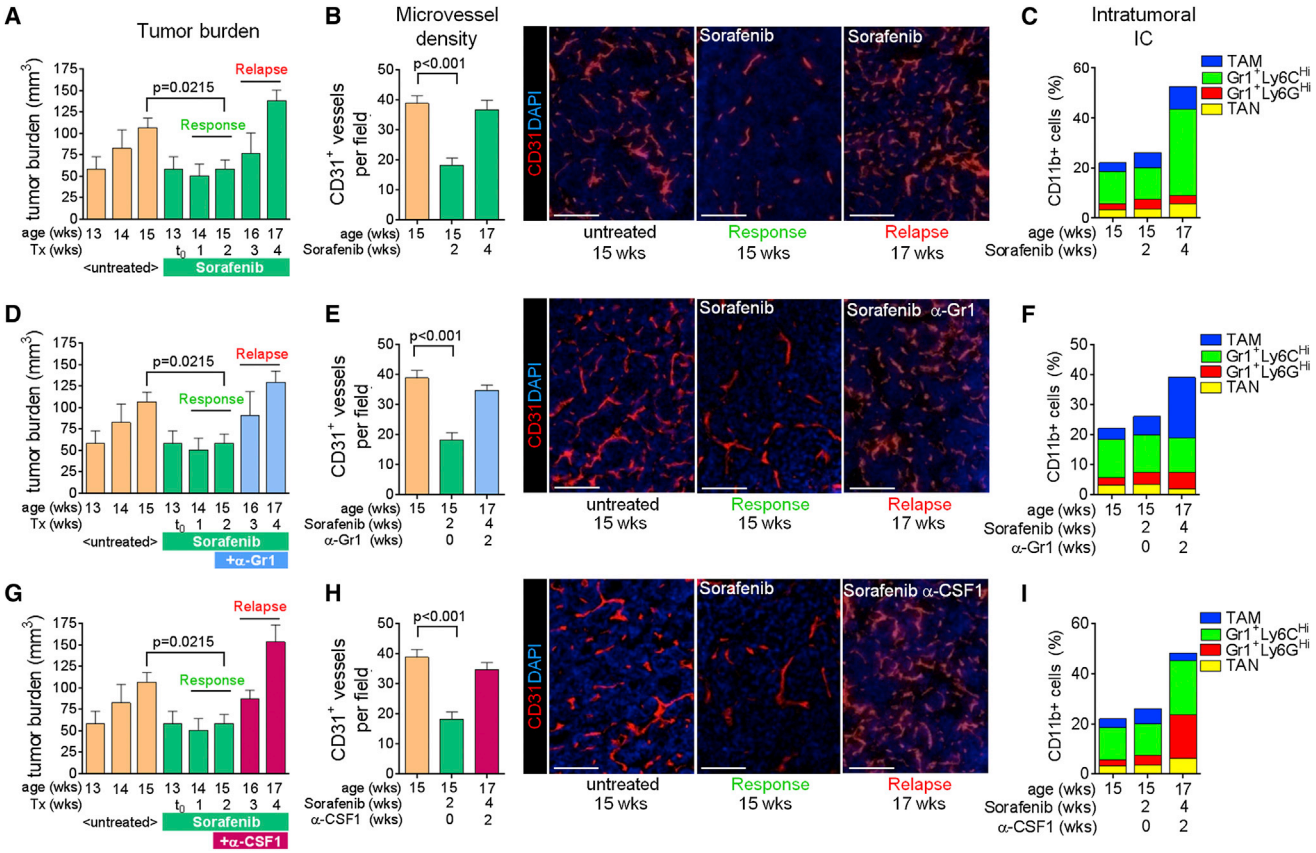

Figure 1. Targeting Distinct Myeloid Populations Induces Compensatory Oscillation

(A) Tumor burden of RT2 mice. Response indicates tumor stasis (2-week sorafenib treatment) and relapse indicates tumor regrowth (4-week sorafenib treatment).

(B) Microvessel density of immunofluorescent anti-CD31-stained tumors.

(C) Myeloid cell composition in RT2 PNET by FACS. $p = 0.0248$ for relapse- versus response-phase Gr1+Ly6C^{Hi} cells.

(D–F) Tumor burden (D), microvessel density (E), and myeloid cell composition (F) in mice treated with sorafenib plus anti-Gr1. $p = 0.01$ for TAM versus sorafenib response-phase TAM; $p = 0.007$ for Gr1+Ly6C^{Hi} cells and TAM versus cognate populations in sorafenib relapse tumors.

(G–I) Tumor burden (G), microvessel density (H), and myeloid cell composition (I) in mice treated with sorafenib plus anti-CSF1. $p < 0.05$ for TAM, Gr1+Ly6C^{Hi}, and Gr1+Ly6G^{Hi} cells versus cognate populations in both sorafenib response- and relapse-phase tumors. Scale bars, 100 μm. Mean ± SEM is presented for all quantitation.

In (D)–(I), data are presented with untreated and sorafenib response tumor data from (A)–(C). See also Figures S1 and S2 and Experimental Proceduresfor details.

rather by the levels of angiostatic chemokines, specifically CXCL14.

Myeloid Cells Regulate Angiogenic Response and Relapse in PNET

We then sought to determine the extent to which intratumoral myeloid cells are the source of intratumoral angiogenic factors. We isolated TAMs, Gr1+Ly6C^{Hi}, and Gr1+Ly6G^{Hi} monocytes, and TAN from RT2 PNET of untreated mice and mice treated for 2 or 4 weeks with sorafenib (alone or in combination with anti-Gr1 or anti-CSF1), and compared their angiogenic gene expression profiles with that of the entire tumor (Figures 2A–2E). Surprisingly, proangiogenic and angiostatic factor gene expression was very similar among all four myeloid populations and reflected that found in whole-tumor extracts. Furthermore, proangiogenic factor gene expression was increased in all four myeloid cell types isolated from responding tumors, and remained unchanged when the tumors became refractory. In contrast, angiostatic CXCL chemokine expression was low in myeloid cells of untreated and relapsing tumors, but was upregulated in cells from responding tumors, with *CXCL14* being the most upregulated factor, followed by *CXCL4* (Figures 2A–2E). Given that expression of all CXCL chemokines was undetectable in CD45+ cell-depleted tumor samples, innate immune cells appear to be the primary source of these chemokines (data not shown). These results have several implications. First, as the angiogenic expression profile of all tumor-associated innate immune cells reflects that of the whole tumor, myeloid cells appear to be the dominant regulators of the angiostatic and proangiogenic status of PNET during antiangiogenic therapy. Second, each myeloid population expressed similar angiogenic factors at comparable levels, arguing that they compensate for each other by redundant expression of these genes. Third, all four innate immune-cell types induced antiangiogenic activities in

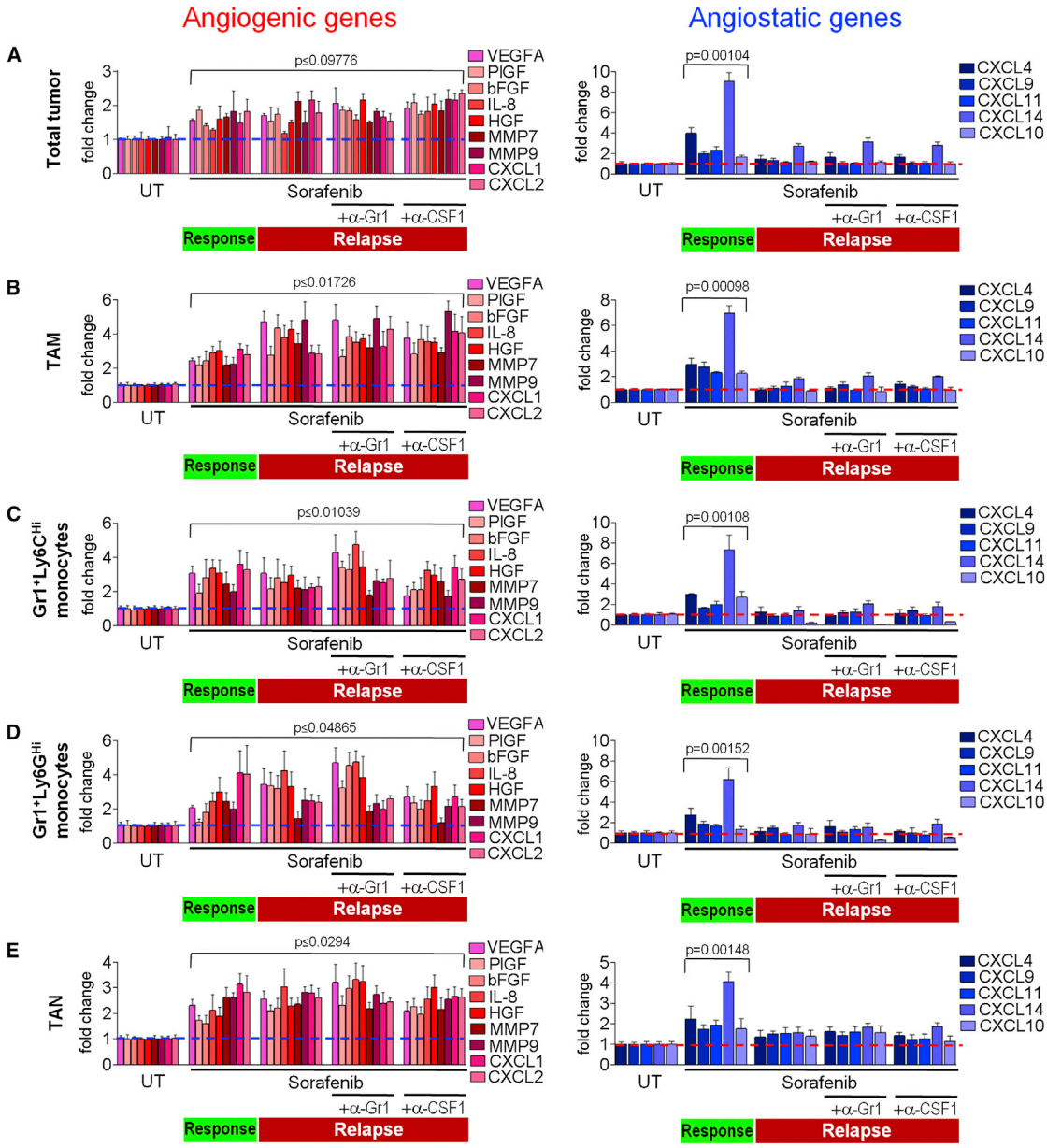

Figure 2. Antiangiogenic Therapy Regulates Both Angiogenic and Angiostatic Gene Expression in Myeloid Cells

(A) qPCR-based expression analyses of proangiogenic and angiostatic genes in RT2 tumors.

(B–E) qPCR expression analysis of FACS-sorted TAMs (B), Gr1+Ly6C^{Hi} monocytes (C), Gr1+Ly6G^{Hi} monocytes (D), and TANs (E) isolated from tumors treated as indicated. Dotted lines indicate baseline gene expression in untreated samples.

Mean ± SEM is presented for quantitation; p values were calculated comparing each treatment group with the untreated (UT) group. See also Figure S3.

responding tumors concomitantly with CXCL14 upregulation, and became proangiogenic in relapsing tumors when they lost their ability to enhance CXCL14 expression.

CXCL14 Thwarts the Angiogenic Activity of Intratumoral Myeloid Cells

Next, we investigated whether blocking CXCL14 would be sufficient to abrogate the antiangiogenic effects of sorafenib in PNET. For this purpose, we used aortic slices cultured ex vivo in the presence of protein extracts made from CD11b+ cells isolated from untreated, 2-week sorafenib-treated (response phase) or 4-week sorafenib-treated (relapse phase) tumors (Figure 3A). Only CD11b+ cells from refractory tumors induced endothelial cell outgrowth and migration from aortic slices (Figure 3A). The addition of a CXCL14-neutralizing antibody rendered CD11b extracts from responding tumors angiogenic, but had no impact on the activities of CD11b extracts from untreated or refractory tumors (Figure 3A). Furthermore, recombinant CXCL14 blocked

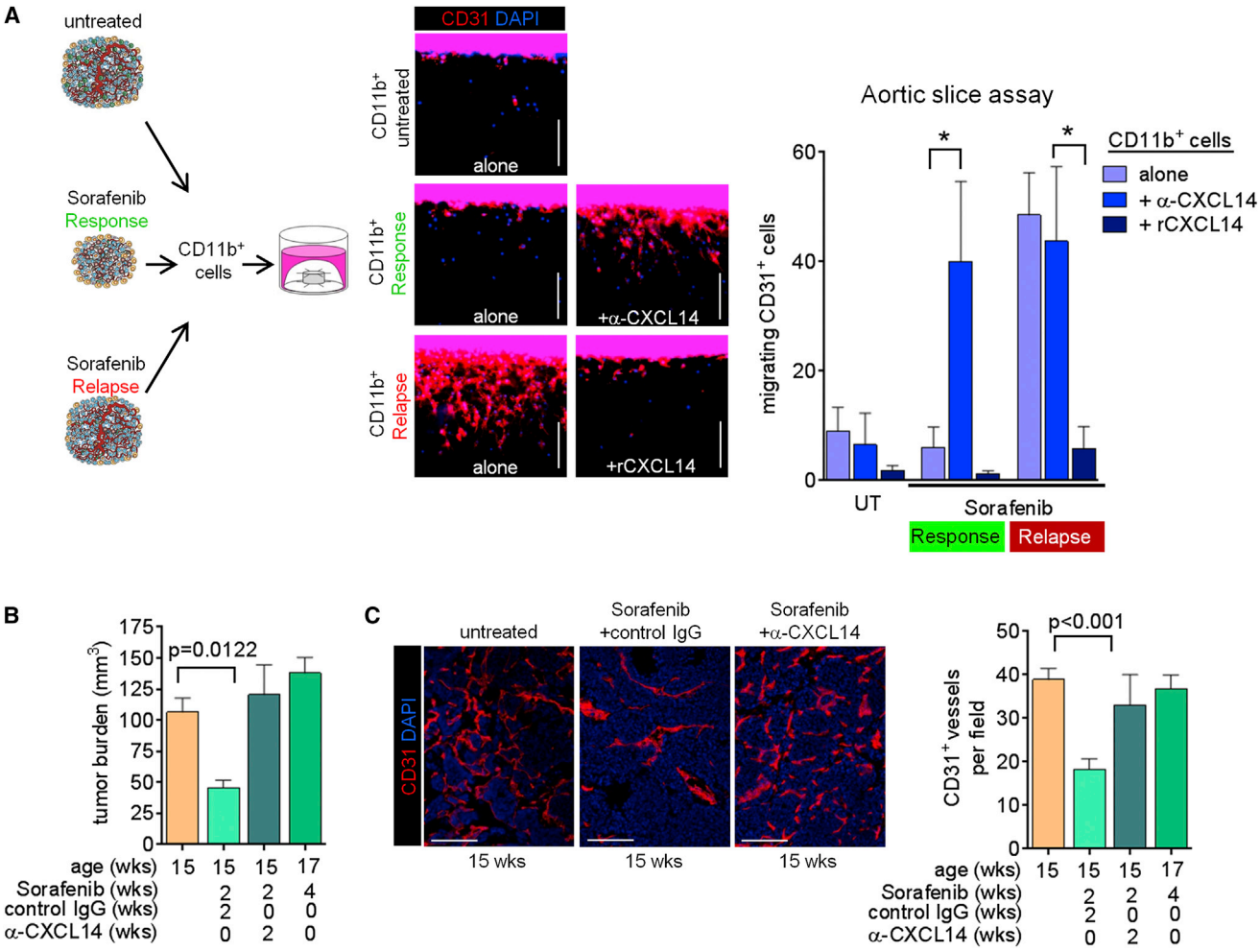

Figure 3. Myeloid CXCL14 Induction Is Necessary for Sorafenib to Elicit an Antiangiogenic Response

(A) Aortic slice assay using CD11b+ cell extracts from untreated and treated RT2 tumors as indicated. Endothelial cell migration from the aortic slice into the surrounding collagen matrix was assessed by immunofluorescent staining of CD31. Quantitation of migrating cells per slice is presented in the right panel. *$p < 0.01$.

(B) Tumor burden of RT2 mice treated with either anti-CXCL14 or control IgG antibody plus sorafenib.

(C) CD31 staining and quantitation of microvessel density of RT2 tumors. Data from untreated mice and mice treated with sorafenib for 4 weeks from Figures 1A and 1B are presented in (B) and (C) for comparison. Mean ± SEM is presented for all quantitation.

the activity of CD11b extracts from refractory tumors (Figure 3A). These results argue that CXCL14 levels determine the angiogenic activity of myeloid cells in PNETs. We then treated RT2 mice with sorafenib in the presence of a neutralizing anti-CXCL14 antibody or control immunoglobulin G (IgG) beginning at 13 weeks of age. Mice that received the control combination exhibited a typical therapeutic response characterized by reduced tumor burden at 15 weeks and a reduction in microvessel density (Figures 3B and 3C). Neutralization of CXCL14, however, abrogated the therapeutic effects of sorafenib, because both tumor burden and microvessel density were comparable to those of untreated mice (Figures 3B and 3C). Thus, myeloid-cell-produced CXCL14 is necessary to induce an antiangiogenic response and must be suppressed to enable a proangiogenic tumor relapse during antiangiogenic therapy.

Antiangiogenic Therapy Promotes an Immune-Stimulating Phenotype in Myeloid Cells during Response that Becomes Immune Suppressive Concomitantly with Tumor Relapse

CXCL14 is not only an angiostatic factor but has also been described to induce dendritic cell maturation, thus stimulating an immune response (Schaerli et al., 2005). As angiogenesis has been found to correlate with immune suppression in different tumors (Motz and Coukos, 2011), we hypothesized that antiangiogenic therapy would change the immune status of tumor-associated myeloid cells, thereby inducing angiostatic activities in these populations. In support of this hypothesis, we found that tumors responding to antiangiogenic therapy exhibited an induction of proinflammatory gene expression and a reduction in immunosuppressive gene expression. In refractory tumors,

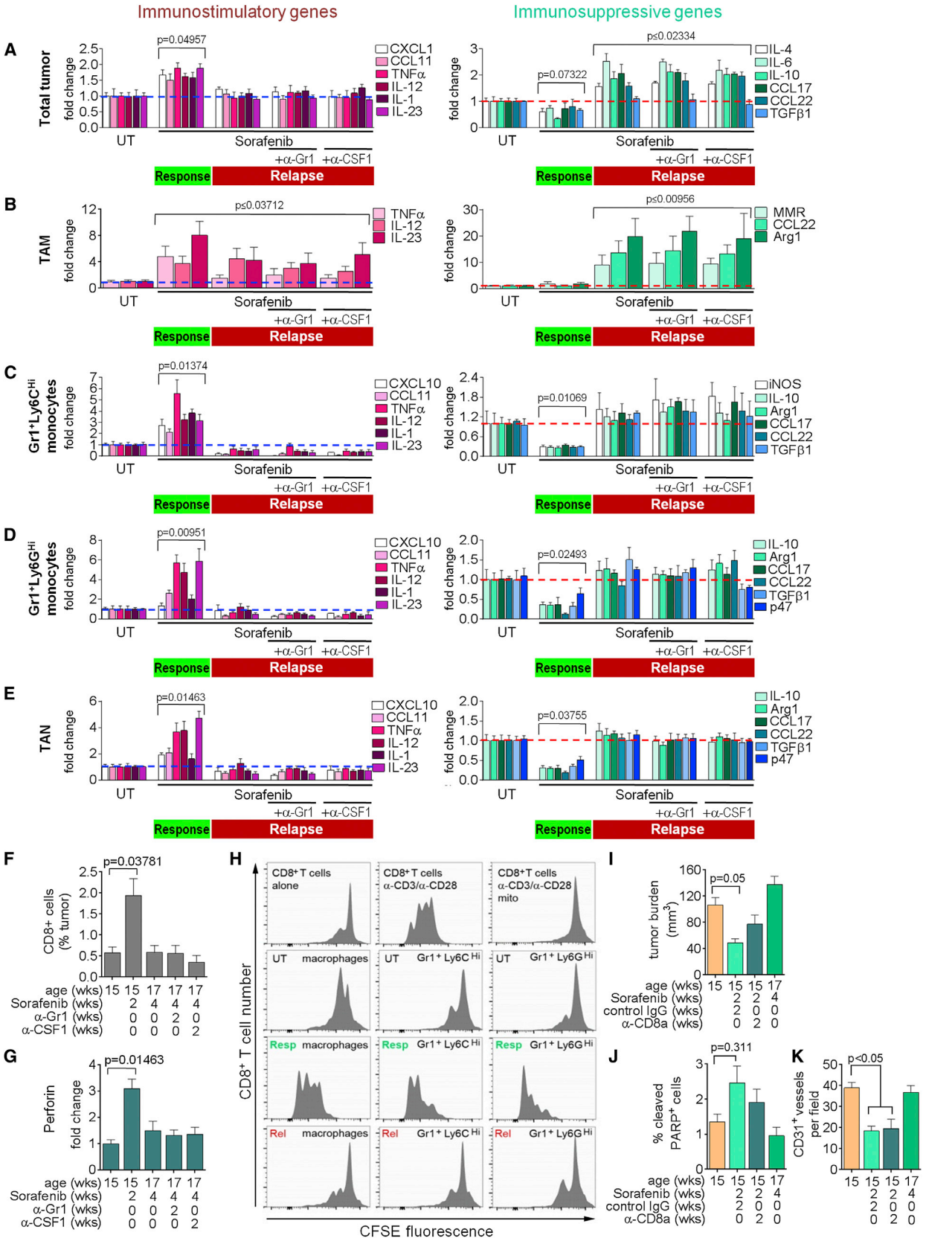

(legend on next page)

proinflammatory gene expression levels went to baseline, whereas the expression of immunosuppressive genes was enhanced (Figures 4A, S4E, and S4F).

To confirm that the changes in inflammatory gene expression in whole tumors were a reflection of those in innate immune cells, we examined the immune expression profile of the four myeloid cell populations isolated from responding and relapsing tumors. Surprisingly, not only TAM and TAN but also both Gr1+ monocyte populations displayed an immune-stimulating phenotype in responding tumors that reverted upon tumor relapse (Figures 4B–4E). TAM exhibited increased expression of the proinflammatory cytokines *IL-12* and *IL-23* and the proinflammatory response gene *TNF*α in responding tumors, which remained elevated, albeit at a lower level, in relapsing tumors. This was counteracted by upregulation of the immunosuppressive factors *MMR*, *CCL22*, and *Arg1* in relapsing tumors (Figure 4B). Similarly to TAM, all Gr1+ populations showed increased expression of proinflammatory genes (*TNF*α, *CCL11*, *IL-12*, and *IL-23*) in responding tumors, which became reduced to or below baseline levels in relapsing tumors. In contrast, expression of immunosuppressive factors, including *IL-10* and *Arg1*, was reduced in all Gr1+ populations from responding tumors and returned to baseline levels upon tumor relapse (Figures 4C–4E).

To validate that the different myeloid cells were immune stimulating in responding tumors and immune suppressive in relapsing tumors, we analyzed T cell numbers and activity. Infiltrating CD8+ cytotoxic T cells (CTLs) increased in tumors responding to therapy and then dropped to levels observed in untreated tumors as the tumors relapsed (Figure 4F). Concomitantly, CD8+ cells isolated from responding tumors, but not from untreated or relapsing tumors, expressed elevated *Perforin* mRNA and Granzyme B protein levels, indicative of activation (Figures 4G and S4A). CD4+ T cells did not change in number during sorafenib treatment, but exhibited lower *IL-10* expression during response, suggesting a reduction in CD4+ regulatory T cells (Figures S4B and S4C).

Next, to test whether the changes in myeloid cell phenotype were responsible for the different T cell behaviors in responding and relapsing tumors, we assessed the ability of myeloid cells to stimulate CD8+ T cell proliferation. Using a coculture assay in which myeloid cells from RT2 spleens were mixed with naive CD8+ T cells, we found that macrophages and Gr1+ monocytes isolated from untreated and relapse-phase RT2 tumors suppressed CD8+ T cell proliferation, whereas response-phase myeloid cells permitted CD8+ T cell proliferation (Figure 4H). We obtained similar results with CD11b+ cells isolated from untreated, responding, or refractory tumors (Figure S4D). These results suggest that CTLs contribute to the therapeutic effects of antiangiogenic therapy. Indeed, CD8+ T cell depletion in RT2 mice resulted in a lower response to sorafenib, as tumor burden was increased and tumor cell apoptosis decreased compared with tumors treated with sorafenib plus IgG control, albeit at statistically nonsignificant levels (Figures 4I and 4J). This intermediate response stemmed from sorafenib's ability to reduce overall vessel density and induce apoptosis in the absence of CTL cells, due to CXCL14 upregulation (Figure 4K).

These results demonstrate that antiangiogenic therapy drives the polarization of TAM, TAN, and both Gr1+ monocytes to an immune-stimulating type, promoting CTL proliferation and activation that coincides with their angiostatic activity, leading to vessel reduction, enhanced tumor cell apoptosis, and subsequent tumor growth blockade. However, this effect is transient, as all four myeloid cell populations become skewed toward an immunosuppressive phenotype in refractory PNETs, leading to immune suppression, reneovascularization, and tumor regrowth.

Activation of PI3K Signaling in Myeloid Cells Promotes Immune Suppression and Reneovascularization during Antiangiogenic Therapy

Our results revealed that myeloid cells in untreated tumors differed from those in relapsing tumors undergoing sorafenib treatment. The myeloid cells were not only increased in relapsing tumors but also displayed elevated levels of immune-suppressive and proangiogenic factors, and lower levels of immune-stimulating molecules compared with myeloid cells in untreated tumors. Thus, we hypothesized that PNETs activate myeloid cells to further promote inflammation and subsequent tumor relapse. Indeed, we identified enhanced levels of tumor-derived growth factors and chemokines, including SDF1α and IL-6 (Figures S5A–S5C) in relapsing tumors. Both SDF1α and IL-6 were previously shown to mediate myeloid infiltration and subsequent tumor progression through activation of PI3Kγ in myeloid cells (Schmid et al., 2011). Congruent with the finding that both γ and δ isoforms of PI3K are immune-cell specific, we found that TAM, TAN, and GR1+ monocytes expressed both isoforms, whereas PNET cells did not (Figure S5D; Hirsch et al., 2000; Rommel et al., 2007). To determine PI3K activation in intratumoral myeloid cells, we assessed the phosphorylation of ribosomal protein S6, a downstream target of PI3K, in CD11b+ cells of untreated and sorafenib-responding and relapsing PNETs (Figures 5A and 5B). While only about 18%–20% of tumor-associated CD11b+ cells exhibited PI3K activity in untreated or responding tumors, up to 80% of myeloid cells were activated in

Figure 4. Antiangiogenic Therapy Induces Myeloid Cell Polarization

(A–E) qPCR RNA analyses of immune-modulating genes from RT2 tumors (A), RT2 tumor-isolated TAMs (B), Gr1+Ly6C^{Hi} (C) and Gr1+Ly6G^{Hi} monocytes (D), and TANs (E) untreated or treated as indicated; p values were calculated by comparing total untreated gene expression.

(F) FACS-analysis of intratumoral CD8+ CTLs.

(G) qPCR analysis of *Perforin* in CD8+ CTLs.

(H) CFSE-based proliferation assay of CD8+ T cells cocultured with splenic myeloid populations from RT2 mice treated as indicated.

(I–K) Tumor burden (I), apoptosis (J), and microvessel density (K) in mice treated concurrently with sorafenib plus anti-CD8a compared with untreated and sorafenib relapse data from Figures 1A and 1B. Mean ± SEM is presented for all quantitations. UT, untreated; Resp, response (2-week sorafenib); Rel, relapse (4-week sorafenib); mito, Mitomycin C.

See also Figure S4 and Supplemental Experimental Procedures for details.

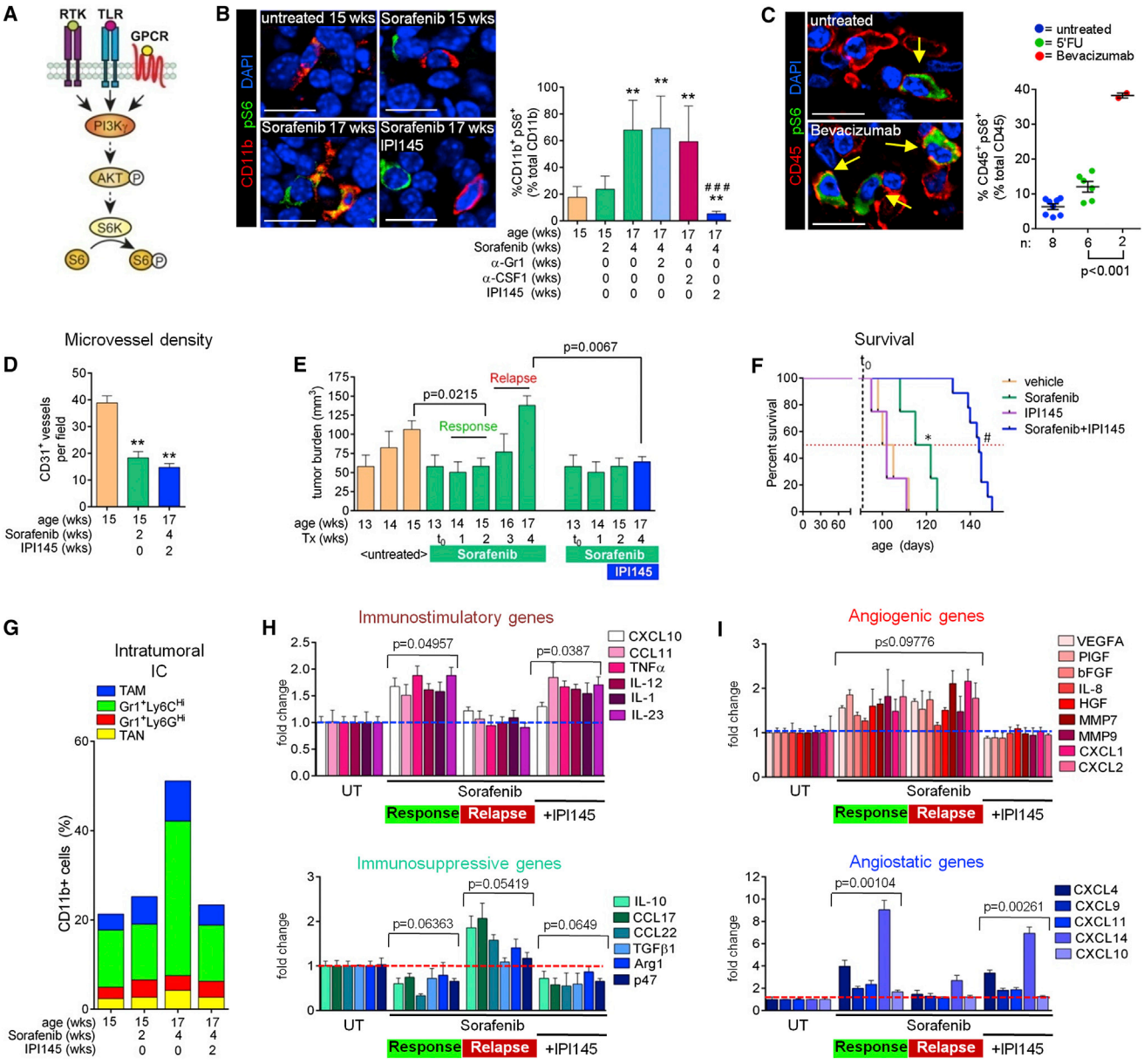

Figure 5. The PI3Kγ/δ Inhibitor IPI145 Enhances the Efficacy of Antiangiogenic Therapy

(A) Key downstream effectors of the PI3K signaling pathway.

(B) pS6 and CD11b immunofluorescent staining in RT2 PNET. Quantitation of CD11b+ pS6+ cells is shown on the right; **p < 0.005 versus sorafenib 2 weeks; ###p < 0.0005 versus sorafenib 4 weeks alone and plus antibodies.

(C) CD45 and pS6 staining and quantitation in PNET samples from patients treated as indicated. Each dot represents one patient. Scale bars, 7.5 μm.

(D and E) Tumor microvessel density (D) and burden (E) from mice treated with sorafenib plus IPI145 versus untreated and sorafenib response-phase tumors from Figures 1A and 1B.

(F) Survival of RT2 mice treated with vehicle (n = 4; median survival = 102 days), sorafenib (n = 4; median survival = 118.5 days), sorafenib plus IPI145 (n = 10; median survival = 144 days), or IPI145 alone (n = 4; median survival = 102 days). ns, no significance versus vehicle. *p = 0.0266 versus vehicle; #p = 0.00068 versus sorafenib. Vertical dashed line indicates the start of sorafenib treatment (91 days); red dotted line indicates 50% survival.

(G) Myeloid cell composition of tumors treated with sorafenib plus IPI145 compared with untreated and sorafenib-treated tumors from Figure 1C. $p \leq 0.05$ for Gr1+Ly6C^{Hi} monocytes and TAM from 4-week sorafenib alone versus 4-week sorafenib plus IPI145.

(H and I) qPCR analyses of immune- (H) or angiogenesis- (I) modulating genes from RT2 tumors. PNETs treated with sorafenib plus IPI145 are compared with untreated and sorafenib-treated tumors from Figure 3A; p values were calculated by comparing each treatment with untreated (UT) samples. Dotted lines indicate baseline gene expression in untreated samples. Mean ± SEM is presented for all quantitations.

See also Figure S5.

relapsing tumors (Figure 5B). Importantly, analysis of human PNET biopsies from naive patients or patients who had been treated with the chemotherapeutic agent 5-FU or bevacizumab until relapse revealed that only patients who had received bevacizumab displayed an increase of activated intratumoral myeloid cells, as visualized by phosphorylated S6 (pS6) staining in CD45+ immune cells, confirming the results in the RT2 PNET model (Figure 5C). These data suggest that PNETs become refractory to antiangiogenic therapy by activating PI3K signaling in myeloid cells.

Inhibiting PI3K in Myeloid Cells Enhances the Efficacy and Endurance of Antiangiogenic Therapy

If induced PI3K signaling mediates an immunosuppressive and proangiogenic switch in myeloid cells that blocks the tumor-inhibitory effects of sorafenib, then inhibition of PI3K activity should suffice to prolong the tumor response. To test this proposition, we pharmacologically blocked PI3K in myeloid cells using the small-molecule inhibitor IPI145, which targets both PI3Kγ and PI3Kδ, and is currently being tested in several clinical trials (e.g., NCT02004522, NCT02049515, and NCT02204982) for hematological malignancies. We first confirmed that IPI145 selectively inhibited myeloid cell proliferation and PI3K-mediated Akt phosphorylation in vitro (Figures S5E and S5F). We then started sorafenib treatment of RT2 mice at 13 weeks of age and added IPI145 to the treatment modality at 15 weeks of age, when the RT2 mice were still responding to sorafenib. After 2 weeks of combined myeloid PI3K inhibition and sorafenib treatment, we confirmed that IPI145 blocked PI3K activity in CD11b+ myeloid cells (Figure 5B). Consequently, IPI145 treatment maintained the low microvessel density observed in tumors responding to sorafenib (Figure 5D) and impaired tumor regrowth (Figure 5E), which nearly doubled the overall survival of the RT2 mice (Figure 5F). Notably, congruent with our observation that myeloid-PI3K activity was low in untreated RT2 PNETs, IPI145 alone had no effect on the survival of the RT2 mice (Figures 5B and 5F). This underscores the notion that in PNETs, PI3K activity is switched on in myeloid cells as a distinct step during therapeutic resistance.

To understand how inhibition of PI3K signaling in myeloid cells enables a sustained response to antiangiogenic therapy, we assessed the composition and status of the tumor-associated myeloid cell populations. Myeloid cells from tumors of RT2 mice treated with sorafenib plus IPI145 revealed a reduction in intratumoral Gr1+Ly6C^{Hi} monocytes and TAM (Figures 5G and S5G). Importantly, IPI145 inhibited both the repression of immune-stimulating gene expression and the induction of immune-suppressing gene expression observed in tumors undergoing relapse during antiangiogenic therapy (Figure 5H). Furthermore, IPI145 reduced the expression of proangiogenic factors and maintained high levels of *CXCL14* and *CXCL4* (Figure 5I). The changes in gene expression profiles directly reflected the effects of IPI145 on myeloid cells because the proinflammatory and angiostatic expression patterns of whole tumors reflected those of TAM, Gr1+Ly6C^{Hi} and Gr1+Ly6G^{Hi} monocytes, and TAN (Figures 6A–6D). Moreover, the immune-stimulating nature of these cells was confirmed by an increase in tumor-associated CTLs and their expression of *Perforin* (Figures 6E and 6F). Altogether, these results confirm that myeloid cells undergo a PI3K-mediated switch to become immune suppressive and proangiogenic, and thus facilitate tumor relapse during antiangiogenic therapy. They also demonstrate that simultaneous inhibition of PI3K signaling in all myeloid cell subtypes overcomes the oscillating resistance observed when distinct myeloid cell subpopulations are targeted.

PI3K-Activated Myeloid Cells in PyMT Tumors Limit the Efficacy of Antiangiogenic Therapy

As PNETs contain a majority of inert CD11b+ cells in which PI3K is inactive, but induce myeloid-PI3K signaling to curtail angiogenesis inhibition, we hypothesized that the number of PI3K-activated myeloid cells could determine the effects of antiangiogenic agents in cancers. To test this proposition, we required a model in which anti-VEGF therapy would be only partially effective. We employed an orthotopic mouse model of breast cancer driven by the MMTV-PyMT transgene, a system that is widely used to study the impact of myeloid cells during tumor progression, together with the anti-VEGFR2 antibody DC101 (DeNardo et al., 2009; Coussens et al., 2013; Mazzieri et al., 2011; Lin et al., 2003). In contrast to the PNET model, antiangiogenic therapy did not produce distinct response or relapse phases in PyMT tumors, but slowed down the pace of growth by 33% (Figure 7A). Analysis of tumors after a 12-day treatment revealed that DC101 reduced microvessel density by 37%, whereas TAN and Gr1+ monocytes increased, leading to a modest elevation of myeloid cells (Figures 7B, 7C, and S7B). Interestingly, as in the RT2 PNETs, anti-Gr1 reduced the number of TAN and Gr1+Ly6G^{Hi} monocytes while increasing intratumoral TAM. Conversely, anti-CSF1 reduced the number of TAM and increased TAN content, displaying again an oscillating pattern of resistance (Figures 7C and S7B). Thus, combinatorial treatment of DC101 with either anti-Gr1 or anti-CSF1 did not reduce tumor growth or vessel density compared with DC101 alone, and neither antibody alone affected tumor growth (Figures 7B and S7A).

Then, we investigated whether the PI3K-activation status in tumor-associated myeloid cells was responsible for the partial response to antiangiogenic therapy. Indeed, analysis of pS6 kinase+ CD11b+ cells in untreated tumors revealed PI3K activation in 46.2% of tumor-associated myeloid cells (Figure 7D), a >2.5-fold higher percentage than what we observed in naive RT2 tumors (Figure 5B). Therefore, IPI145 alone elicited an intermediate response. DC101 treatment also produced an intermediate response, but nearly doubled the population of PI3K-activated myeloid cells (Figure 7D). Congruently, we found that DC101 induced expression of the immunosuppressive genes *IL-10* and *TGFβ1* as early as 4 days after the start of therapy, without affecting expression of the proinflammatory genes *IL-23* and *TNFα* (Figure 7H). Further, as in the PNET model, DC101 induced expression of the proangiogenic genes *VEGF* and *bFGF* concomitantly with an increase in expression of both *CXCL14* and *CXCL4* (Figure 7I). These data suggest that the immune-suppressive and proangiogenic activities of PI3K-activated myeloid cells outweigh the immune-stimulatory and angiostatic activities of the PI3K-nonactive myeloid cells, thus explaining the intermediate response to antiangiogenic therapy (Figures 7H and 7I). Therefore, blocking PI3K in myeloid cells should be sufficient to

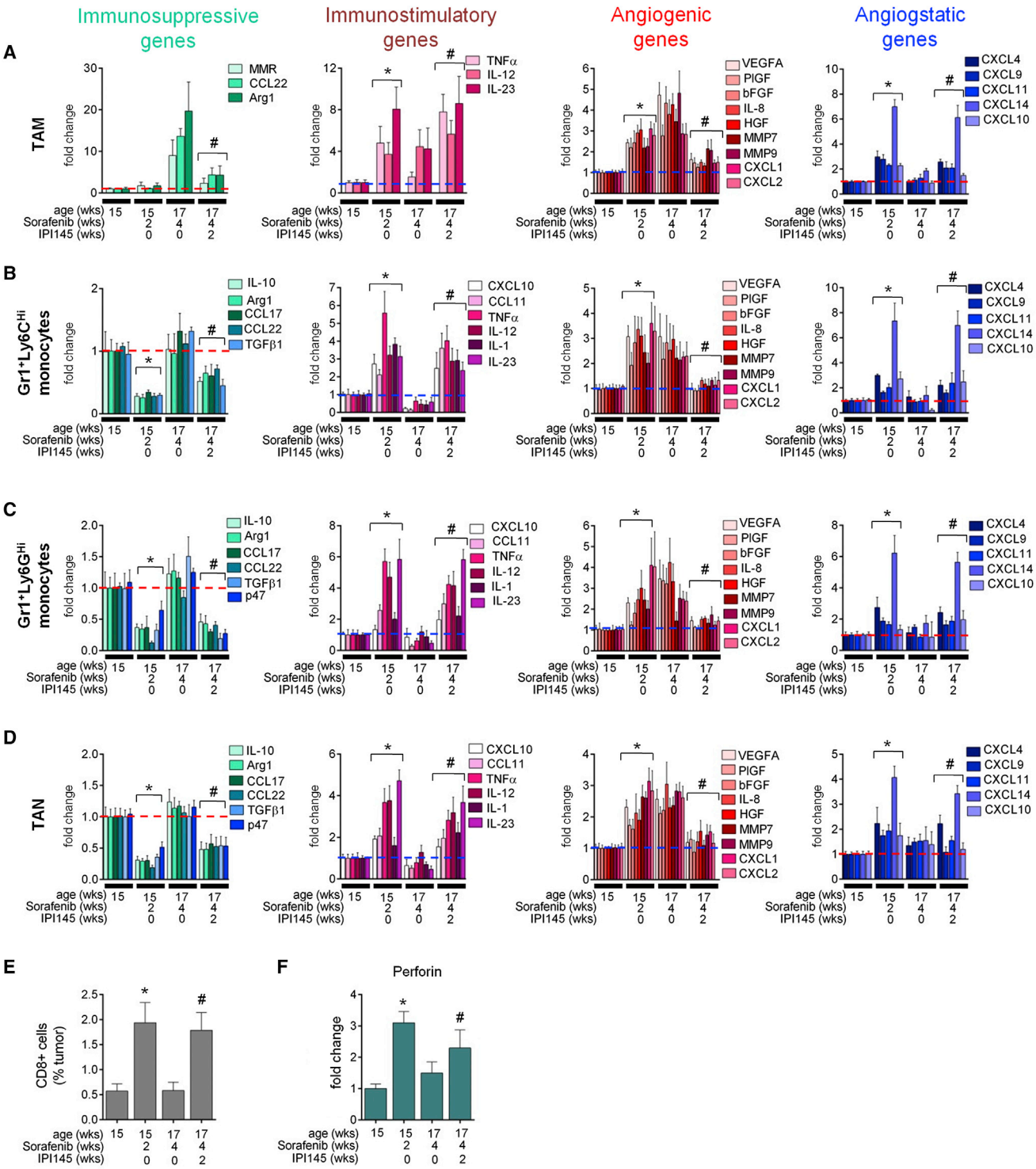

Figure 6. IPI145 Induces Immune Stimulatory and Angiostatic Factors in Myeloid Cells during Antiangiogenic Therapy

(A–D) qPCR analyses of TAMs (A), Gr1+Ly6C^{Hi} (B) and Gr1+Ly6G^{Hi} monocytes (C), and TANs (D) from tumors of RT2 mice treated with sorafenib plus or minus IPI145; p values were calculated comparing each treatment group to untreated (UT).

(E) CD8+ CTLs from tumors of mice treated with sorafenib plus IPI145.

(F) *Perforin* expression in CD8+ CTLs from tumors of mice treated with sorafenib plus IPI145. Dotted lines indicate baseline gene expression in untreated samples. *p $\leq$ 0.05 versus untreated; #p $\leq$ 0.05 versus 4 week sorafenib alone. Data from untreated and sorafenib-treated tumors from Figures 2B–2E and 4B–4G are presented in (A)–(F) for comparison. Mean ± SEM is presented for all quantitation.

increase the sensitivity of PyMT tumors to DC101. Of note, similarly to the PNET cells, PyMT breast tumor cells did not express detectable levels of *PI3K*γ or *PI3K*δ, and did not respond to IPI145 in vitro (Figures S7D and S7E). Indeed, we found that combining IPI145 with DC101 substantially reduced the number of tumor-associated pS6+ CD11b+ cells to 9% (Figure 7D). This corresponded to a reduction in tumor growth, with a further trend in microvessel density reduction concomitant with enhanced immune-stimulatory and reduced immune-suppressive gene expression profiles (Figures 7E, 7F, 7H, and 7I). IPI145 decreased the levels of intratumoral TAM, Gr1+ monocytes, and TAN compared with both control and DC101-treated tumors (Figures 7G and S7C), and further enhanced *CXCL4* and *CXCL14* expression, similar to the results observed in the PNET model (Figure 7I). As expected, IPI145 repressed DC101-induced expression of *IL-10* and *TGF*β*1*, and induced *IL-23* and *TNF*α expression in TAM, Gr1+ monocytes, and TAN (Figures S6A–S6D). Furthermore, it enhanced *CXCL4* and *CXCL14* expression in these populations and repressed DC101-induced *VEGF* and *bFGF* transcription (Figures S6A–S6D). Consequently, IPI145 induced *Perforin* expression in tumor-associated CTLs (Figures S6E and S6F). Thus, in the PyMT and PNET models, PI3K activation in myeloid cells hindered the efficacy of antiangiogenic therapy by promoting immune suppression and limiting the expression of angiostatic factors. These results not only demonstrate that oscillating immune cells activate PI3K signaling to mediate resistance, but also suggest that the extent of PI3K-activated myeloid cells may predict tumor response to antiangiogenic therapy.

DISCUSSION

In this study, we demonstrated that intratumoral myeloid cells dynamically drive responsiveness as well as resistance to angiogenic inhibitors targeting the VEGF/VEGFR pathway. Sorafenib and DC101 skewed different inert CD11b+ myeloid cell populations, including TAM, TAN, and Gr1+Ly6C^{Hi} and Ly6G^{Hi} monocytes, to an immune-stimulatory and angiostatic phenotype in tumors by enhancing their expression of the angiostatic and immune-stimulatory chemokine CXCL14 (and to a lesser extent CXCL4). Surprisingly, the efficacy of the VEGF/VEGFR inhibitors depended on the induction of these myeloid CXCL chemokines rather than on direct inhibition of VEGFR signaling in endothelial cells. Although depleting CTL cells during antiangiogenic therapy in RT2 mice lowered the apoptotic rate without affecting vessel density, blocking CXCL14 was sufficient to disable both the reduction in vessel density and enhanced tumor cell apoptosis, thereby completely abrogating the ability of sorafenib to promote tumor stasis. While CXCL4 is believed to induce antiangiogenic activity by interfering with integrins on the surface of endothelial cells (Aidoudi et al., 2008; Maione et al., 1990; Sharpe et al., 1990), less is known about the mechanism underlying the antiangiogenic activity of CXCL14, although CXCL14 is known for its effects on dendritic cell maturation (Shellenberger et al., 2004). Other CXCL chemokines, such as CXCL9 and CXCL10, have also been identified in macrophages that exert angiostatic functions, implying a myeloid-specific angiostatic signature (Mantovani et al., 2005). Our findings reveal the necessity of using myeloid cells in antiangiogenic therapy, and show that the proangiogenic capacity observed in immunosuppressive myeloid populations does not stem from the enhanced expression of angiogenic factors, but rather from the repression of angiostatic CXCL chemokines that also elicit immune-stimulating functions.

In order to reinitiate angiogenesis and immune suppression, tumors induced infiltration of Gr1+ monocytes and neutrophils, and produced factors that activated the PI3K signaling axis in all CD11b+ immune cells. This rendered myeloid cells nonresponsive to angiogenesis inhibitors and increased their proangiogenic and immune-suppressive properties (Figures 7J and 7K). Our findings further reveal that the PI3K-activation status of myeloid cells in tumors determines the efficacy of antiangiogenic therapy. In naive PNETs, most myeloid cells were inactive, leading to a pronounced antiangiogenic effect; however, in PyMT tumors, with more than 40% myeloid PI3K activity, therapy only partially impaired angiogenesis and tumor growth.

Interestingly, targeting the enhanced influx of Gr1+ cells was not sufficient to prolong the response to angiogenic blockade in both tumor models, as it resulted in an increase in TAM concomitant with enhanced intratumoral M-CSF levels. Targeting TAM induced an increase in Gr1+ cells due to elevated G-CSF levels (Figures S2D–S2F), leading to an oscillating pattern of distinct immune cell populations. Chemotherapeutics are commonly given in conjunction with antiangiogenic agents and have been shown to modulate immune suppression (Coussens et al., 2013). However, addition of the chemotherapeutic temolozolomide (TMZ) did not affect either the oscillating compensation of myeloid cells when TAM or Gr1+ cells were targeted during antiangiogenic therapy or the timing of the angiogenic relapse, although it further reduced tumor burden by about 30% (Figures S2G–S2I). Further evidence for oscillating resistance comes from a previous study in which genetic depletion of TAMs (the major source of the proangiogenic enzyme MMP9) in a transgenic mouse model of cervical cancer resulted in a compensatory increase in TAN, which then became the primary source of MMP9, promoting neovascularization (Pahler et al., 2008). Furthermore, various approaches to deplete TAM in models of thyroid, cervical, and pancreatic cancers have also been shown to increase tumor-associated Gr1+ cells (Mitchem et al., 2013; Ryder et al., 2013). Interestingly, however, Gr1+ cells in the absence of TAM could not compensate for the TAM-dependent maintenance of the ALDH+ cancer stem cell fraction in PDAC (Mitchem et al., 2013) or the growth deficiency of Braf-driven thyroid tumors (Ryder et al., 2013). Taken together, these results support the notion that innate immune cells share functions in angiogenesis and immune modulation, likely to maintain tissue homeostasis, but also have distinct and noncompensatory functions in other areas such as stemcellness, invasion, and metastasis (Mitchem et al., 2013; Qian and Pollard, 2010; Yang et al., 2008).

Furthering the concept of functional redundancies among tumor-infiltrating myeloid cells in angiogenesis and immune suppression, we identified two Th2-skewed myeloid phenotypes (simplistically referred to as "M2"-like) that differed in their PI3K-activation status (Figures 7J and 7K). Whereas PI3K-inert myeloid cells expressed several proangiogenic factors and lacked immune-stimulating activity (M2 cells), myeloid cells with active PI3K signaling aggravated angiogenic and immune-

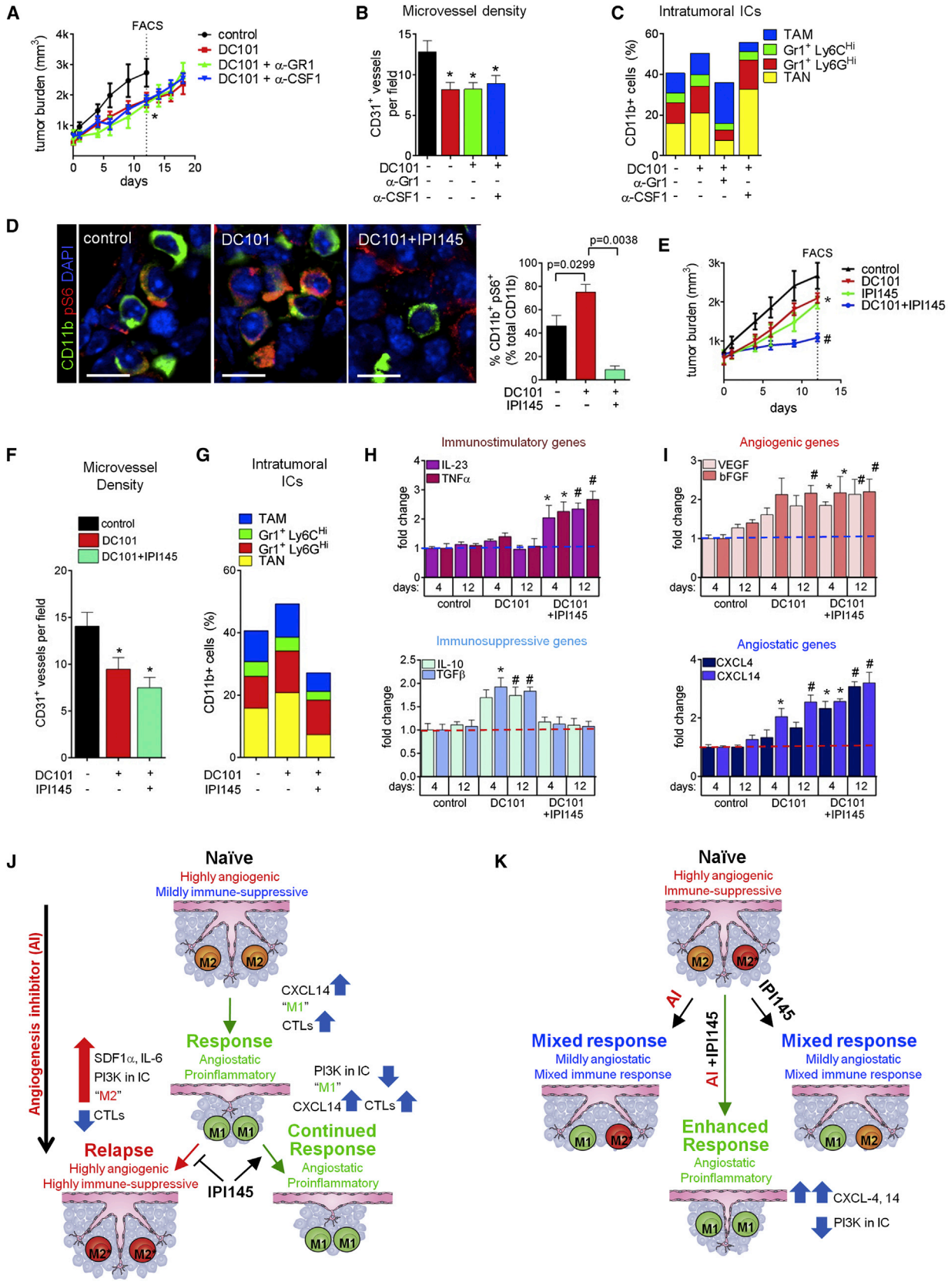

(legend on next page)

suppressive activities, and thwarted the immune-stimulatory and angiostatic conversion by VEGF/VEGFR inhibitors (M2* cells). Interestingly, M2* cells exhibited an expression profile, including increased MMR (MRC1) levels, that was in part reminiscent of a Tie2-expressing monocyte (TEM) signature (Pucci et al., 2009; Squadrito et al., 2012). TEMs are a subpopulation of TAMs that exhibit exacerbated angiogenic activity and were also found to accumulate in relapsing tumors undergoing anti-VEGFR therapy (Rigamonti et al., 2014). Therefore, it is intriguing to speculate that the TEM signature is in part regulated by macrophage PI3K activation.

In contrast to epithelial cells and cancer cells, myeloid cells specifically express the γ and δ isoforms of PI3K, which can be blocked with IPI145. Although we did not differentiate between PI3Kγ and PI3Kδ activity, PI3Kγ is highly enriched in myeloid cells, where it transduces GPCR, TLR, and RTK signaling to facilitate myeloid cell infiltration to inflammatory sites and evoke inflammatory responses in tumors and other diseases (González-García et al., 2010; Hirsch et al., 2000; Schmid et al., 2011), suggesting that the γ isoform is the major regulator of tumor inflammation in myeloid cells. Several tumor-derived chemoattractants have been described to activate PI3Kγ signaling (Schmid et al., 2011; Hirsch et al., 2000). Among these, we found IL-6 and SDF1α to be upregulated in relapsing PNETs. As *SDF1α* and *IL-6* are hypoxia-regulated genes, it is conceivable that microenvironmental changes, such as therapy-induced hypoxia, promote such a conversion. Indeed, macrophage polarization is regulated in part by intratumoral hypoxia, in which Semaphorin 3A/Neuropilin-1 signaling enables the infiltration of myeloid cells into hypoxic areas in which they secrete various immune-suppressive and proangiogenic factors (Casazza et al., 2013; De Palma and Lewis, 2013; Qian and Pollard, 2010).

Together, these data provide a rational basis for future therapeutic modalities to combine antiangiogenic and immune therapies to generate more durable effects and likely sensitize resistant tumors to antiangiogenic therapy. This is further supported by observations that the abnormal tumor vasculature fosters an immune-suppressive microenvironment that enables tumors to evade host immunosurveillance (Motz and Coukos, 2013). In addition, the proangiogenic factor VEGF not only suppresses the function of various immune cells but also diminishes leukocyte-endothelial interactions, thereby hindering infiltration of immune T-effector cells into the tumor (Bouzin et al., 2007; Gabrilovich et al., 1996; Griffioen et al., 1996; Motz and Coukos, 2011). Congruently, VEGF blockade was recently found to result in TAM polarization toward an immune-supporting state and increased T cell infiltration into tumors by creating an even distribution of patent vessels that reduced tumor hypoxia (Huang et al., 2012), whereas genetic deletion of Rgs5 in pericytes increased T cell infiltration into tumors and enhanced survival after adoptive T cell transfer by normalizing the tumor vasculature (Hamzah et al., 2008).

The existence of oscillating innate immune cells to convey reneovascularization supports the idea of modulating the overall immune response to control tumor growth, as opposed to targeting distinct myeloid populations, because this approach would not leave behind nontargeted myeloid cells able to foster tumor reneovascularization. We found that PI3K inhibition in all myeloid cells generated an enduring angiostatic and immune-stimulatory environment in which antiangiogenic therapy remained efficient. Other approaches to reverse immune suppression, including blockade of self-tolerance checkpoints, are showing increasing promise, with the anti-CTLA-4 antibody ipilimumab having already received FDA approval for advanced melanoma. Various antiangiogenic immune therapies have been tested in the clinic, more recently in combination with checkpoint blockers, with encouraging results (Garber, 2014; Schoenfeld and Dranoff, 2011). Ongoing and future studies will reveal whether combining antiangiogenic therapies with these new immune-modulating strategies will more robustly inhibit tumor angiogenesis and promote an enduring immune-stimulatory milieu that could lead to prolonged survival in cancer patients.

Figure 7. Myeloid PI3K Limits Antiangiogenic Therapy in PyMT Tumors

(A) PyMT tumor growth. *$p < 0.05$ for treatment groups versus control at day 12. Data represent at least six mice per group.

(B) Microvessel density of tumors at day 12 of treatment.*$p < 0.05$ versus control.

(C) Intratumoral myeloid cell composition at day 12 of treatment. $p < 0.05$ for TAM, Gr1+Ly6G^{Hi} monocytes, and TAN from DC101 alone versus DC101 plus anti-Gr1; $p < 0.05$ for TAM and TAN from DC101 versus DC101 plus anti-CSF1 at 12 days.

(D) CD11b+ pS6 staining and quantification of PyMT tumors. Scale bars, 5 μm.

(E) Tumor growth in mice treated with IPI145 as indicated. *$p < 0.05$ for DC101, IPI145 versus control at day 12; #$p < 0.05$ for DC101 plus IPI145 versus DC101 at day 12. Data represent at least six mice per group.

(F and G) Microvessel density (F) and myeloid cell composition (G) in tumors after 12 days of treatment. *$p < 0.05$ versus control at 12 days. $p < 0.05$ for TAM and TAN in DC101 plus IPI145 versus cognate populations in DC101 alone.

(H and I) qPCR analyses of immune- (H) and angiogenesis- (I) modulating genes (H) after 4 and 12 days of therapy. *$p < 0.05$ versus 4-day control; #$p < 0.05$ versus 12-day control. Dotted lines indicate baseline gene expression in control samples. Mean ± SEM is presented for all quantitations.

(J and K) Summary of responses to antiangiogenic therapy in RT2 (J) and PyMT (K) models.

(J) Myeloid cells in naive RT2 PNET exhibit a "PI3K-off" M2 phenotype. Angiogenesis inhibitors skew myeloid cells toward a CXCL14-expressing M1 phenotype, which promotes tumor response by impeding angiogenesis and facilitating antitumor immunity. In turn, tumors activate myeloid PI3K signaling, likely by increasing SDF1α and IL-6. PI3K-activated myeloid cells display a highly angiogenic and immune-suppressive M2* phenotype. M2* myeloid cells convey resistance to therapy by blocking antitumor immunity and promoting angiogenesis. IPI145 blocks acquisition of the M2* phenotype, resulting in a sustained tumor response.

(K) Myeloid cells within PyMT tumors are both M2 and M2*. Antiangiogenic therapy alone skews M2 cells toward an M1 phenotype without affecting M2* cells, while IPI145 alone converts M2* cells to an M1 phenotype and does not influence M2 cells. Thus, either treatment elicits only partial responses, whereas combining angiogenesis inhibitors and IPI145 results in conversion of both M2 and M2* cells to the M1 phenotype, thereby enhancing the tumor response.

See Discussion for details and also Figures S6 and S7.

EXPERIMENTAL PROCEDURES

For more details regarding the materials and methods used in this work, see the Supplemental Experimental Procedures.

Tumor Models

RT2 mice (previously described in Hanahan, 1985) were maintained as heterozygotes in the C57BL/6 background. Sorafenib treatment with or without TMZ was initiated at 13 weeks of age and administered until the mice reached the age of 15 weeks or 17 weeks. Mice were treated with anti-Gr1, anti-CSF1, or IPI145 (Active Biochem) beginning at 15 weeks, 2 weeks after initiating sorafenib treatment. For PyMT experiments, syngeneic PyMT breast tumor cells were implanted into the fourth mammary fat pads of female FVB mice at 4–5 weeks of age. Tumors reached 5 mm in diameter before DC101 treatment was initiated alone or in combination with anti-Gr1 or anti-CSF1. All animal studies were reviewed and approved by the UCSF Institutional Animal Care and Use Committee. For more experimental details, see the Supplemental Experimental Procedures.

Human PNET Specimens

Immune cells were assessed for pS6 staining by a neuropathologist (D.M.) in 34 deidentified tumor samples from Hospices Civils de Lyon, representing naive-treated patients and patients treated with 5-FU or bevacizumab. To confirm this assessment, immunofluorescent staining for CD45 and pS6 was performed blindly on tumor samples corresponding to eight untreated patients, six patients treated with 5-FU, and two patients treated with bevacizumab.

Expression Analysis

qPCR expression analyses were performed using whole-tumor or FACS-sorted cell populations and the indicated primer sets. Relative gene expression was calculated as previously described (Livak and Schmittgen, 2001). In brief, L19 was used as a housekeeping gene to generate ΔCt. ΔCt values from untreated mice were used as reference for treatment groups to generate ΔΔCt, and relative gene expression was calculated as $2^{(-\Delta\Delta Ct)}$. Analyses of sorted cells from RT2 mice were performed using at least eight experimental mouse replicates, and whole-tumor analyses were performed using five experimental replicates. Analyses of sorted cells from PyMT tumors as well as whole PyMT tumors were performed using at least six experimental mouse replicates. All reactions were run in triplicate. For primer sequences, see the Supplemental Experimental Procedures.

Statistical Analyses

Statistical analyses were performed under the guidance of the Helen Diller Family Comprehensive Cancer Center Biostatistics and Computational Biology Core. For mouse studies, p values for RT2-PNET and PyMT tumor burdens were calculated using the Wilcoxon rank sum test. The p values for microvessel density, multicolor flow cytometry, CD11b/pS6 and CD45/pS6 immunostaining, and CD8+ T cell content were also calculated using the Wilcoxon rank sum test. This same test was used to evaluate survival (since uncensored). For gene expression analyses, where the transformed signals were more Gaussian and the sample sizes were smaller, comparisons between experimental and control mice for single genes were made using a two-sample t test. To determine whether a signature (e.g., immune response or angiogenesis) was present, p values were added across genes. For this purpose, Fisher's inverse chi-square method was utilized.

SUPPLEMENTAL INFORMATION

Supplemental Information includes Supplemental Experimental Procedures and seven figures and can be found with this article online at http://dx.doi.org/10.1016/j.celrep.2015.03.055.

AUTHOR CONTRIBUTIONS

L.B.R. and G.B. designed research and wrote and edited manuscript. L.B.R. conducted experiments. D.M. and V.H. procured human PNET tissues. M.F. provided anti-CXCL14 antibodies and E.B. provided a clinical perspective. G.B. supervised research.

ACKNOWLEDGMENTS

We thank Jairo Barreto and Lourdes Adriana Esparza for mouse husbandry, genotyping, and drug administration; Bill Hyun for help with multicolor flow cell sorting; Binh Tuyen and Kathrik Kadalabalu Matha for technical assistance; and Drs. Lisa Coussens, Jeff Pollard, Kevan Shokat, Judy Varner, and Ruth Ganss for helpful discussions. This work was supported by grants from the NIH (RO1 CA099948 and U54CA163155 to G.B., and T32CA108462-09 to L.R.) and the AACR Carcinoid Foundation.

Received: September 30, 2014
Revised: January 2, 2015
Accepted: March 25, 2015
Published: April 16, 2015

REFERENCES

Aidoudi, S., Bujakowska, K., Kieffer, N., and Bikfalvi, A. (2008). The CXC-chemokine CXCL4 interacts with integrins implicated in angiogenesis. PLoS ONE *3*, e2657.

Bergers, G., and Hanahan, D. (2008). Modes of resistance to anti-angiogenic therapy. Nat. Rev. Cancer *8*, 592–603.

Bouzin, C., Brouet, A., De Vriese, J., Dewever, J., and Feron, O. (2007). Effects of vascular endothelial growth factor on the lymphocyte-endothelium interactions: identification of caveolin-1 and nitric oxide as control points of endothelial cell anergy. J. Immunol. *178*, 1505–1511.

Casanovas, O., Hicklin, D.J., Bergers, G., and Hanahan, D. (2005). Drug resistance by evasion of antiangiogenic targeting of VEGF signaling in late-stage pancreatic islet tumors. Cancer Cell *8*, 299–309.

Casazza, A., Laoui, D., Wenes, M., Rizzolio, S., Bassani, N., Mambretti, M., Deschoemaeker, S., Van Ginderachter, J.A., Tamagnone, L., and Mazzone, M. (2013). Impeding macrophage entry into hypoxic tumor areas by Sema3A/Nrp1 signaling blockade inhibits angiogenesis and restores antitumor immunity. Cancer Cell *24*, 695–709.

Coussens, L.M., Tinkle, C.L., Hanahan, D., and Werb, Z. (2000). MMP-9 supplied by bone marrow-derived cells contributes to skin carcinogenesis. Cell *103*, 481–490.

Coussens, L.M., Zitvogel, L., and Palucka, A.K. (2013). Neutralizing tumor-promoting chronic inflammation: a magic bullet? Science *339*, 286–291.

De Palma, M., and Lewis, C.E. (2013). Macrophage regulation of tumor responses to anticancer therapies. Cancer Cell *23*, 277–286.

De Palma, M., Venneri, M.A., Galli, R., Sergi Sergi, L., Politi, L.S., Sampaolesi, M., and Naldini, L. (2005). Tie2 identifies a hematopoietic lineage of proangiogenic monocytes required for tumor vessel formation and a mesenchymal population of pericyte progenitors. Cancer Cell *8*, 211–226.

DeNardo, D.G., Barreto, J.B., Andreu, P., Vasquez, L., Tawfik, D., Kolhatkar, N., and Coussens, L.M. (2009). CD4(+) T cells regulate pulmonary metastasis of mammary carcinomas by enhancing protumor properties of macrophages. Cancer Cell *16*, 91–102.

Du, R., Lu, K.V., Petritsch, C., Liu, P., Ganss, R., Passegué, E., Song, H., Vandenberg, S., Johnson, R.S., Werb, Z., and Bergers, G. (2008). HIF1alpha induces the recruitment of bone marrow-derived vascular modulatory cells to regulate tumor angiogenesis and invasion. Cancer Cell *13*, 206–220.

Fischer, C., Jonckx, B., Mazzone, M., Zacchigna, S., Loges, S., Pattarini, L., Chorianopoulos, E., Liesenborghs, L., Koch, M., De Mol, M., et al. (2007). Anti-PlGF inhibits growth of VEGF(R)-inhibitor-resistant tumors without affecting healthy vessels. Cell *131*, 463–475.

Fridlender, Z.G., Sun, J., Kim, S., Kapoor, V., Cheng, G., Ling, L., Worthen, G.S., and Albelda, S.M. (2009). Polarization of tumor-associated neutrophil phenotype by TGF-beta: "N1" versus "N2" TAN. Cancer Cell *16*, 183–194.

Gabrilovich, D.I., Chen, H.L., Girgis, K.R., Cunningham, H.T., Meny, G.M., Nadaf, S., Kavanaugh, D., and Carbone, D.P. (1996). Production of vascular endothelial growth factor by human tumors inhibits the functional maturation of dendritic cells. Nat. Med. *2*, 1096–1103.

Garber, K. (2014). Promising early results for immunotherapy-antiangiogenesis combination. J. Natl. Cancer Inst. *106*, 106.

Giraudo, E., Inoue, M., and Hanahan, D. (2004). An amino-bisphosphonate targets MMP-9-expressing macrophages and angiogenesis to impair cervical carcinogenesis. J. Clin. Invest. *114*, 623–633.

González-García, A., Sánchez-Ruiz, J., Flores, J.M., and Carrera, A.C. (2010). Phosphatidylinositol 3-kinase gamma inhibition ameliorates inflammation and tumor growth in a model of colitis-associated cancer. Gastroenterology *138*, 1374–1383.

Griffioen, A.W., Damen, C.A., Martinotti, S., Blijham, G.H., and Groenewegen, G. (1996). Endothelial intercellular adhesion molecule-1 expression is suppressed in human malignancies: the role of angiogenic factors. Cancer Res. *56*, 1111–1117.

Hamzah, J., Jugold, M., Kiessling, F., Rigby, P., Manzur, M., Marti, H.H., Rabie, T., Kaden, S., Gröne, H.J., Hämmerling, G.J., et al. (2008). Vascular normalization in Rgs5-deficient tumours promotes immune destruction. Nature *453*, 410–414.

Hanahan, D. (1985). Heritable formation of pancreatic beta-cell tumours in transgenic mice expressing recombinant insulin/simian virus 40 oncogenes. Nature *315*, 115–122.

Hirsch, E., Katanaev, V.L., Garlanda, C., Azzolino, O., Pirola, L., Silengo, L., Sozzani, S., Mantovani, A., Altruda, F., and Wymann, M.P. (2000). Central role for G protein-coupled phosphoinositide 3-kinase gamma in inflammation. Science *287*, 1049–1053.

Huang, Y., Yuan, J., Righi, E., Kamoun, W.S., Ancukiewicz, M., Nezivar, J., Santosuosso, M., Martin, J.D., Martin, M.R., Vianello, F., et al. (2012). Vascular normalizing doses of antiangiogenic treatment reprogram the immunosuppressive tumor microenvironment and enhance immunotherapy. Proc. Natl. Acad. Sci. USA *109*, 17561–17566.

Kerbel, R.S. (2008). Tumor angiogenesis. N. Engl. J. Med. *358*, 2039–2049.

Lin, E.Y., Jones, J.G., Li, P., Zhu, L., Whitney, K.D., Muller, W.J., and Pollard, J.W. (2003). Progression to malignancy in the polyoma middle T oncoprotein mouse breast cancer model provides a reliable model for human diseases. Am. J. Pathol. *163*, 2113–2126.

Lin, E.Y., Li, J.F., Gnatovskiy, L., Deng, Y., Zhu, L., Grzesik, D.A., Qian, H., Xue, X.N., and Pollard, J.W. (2006). Macrophages regulate the angiogenic switch in a mouse model of breast cancer. Cancer Res. *66*, 11238–11246.

Livak, K.J., and Schmittgen, T.D. (2001). Analysis of relative gene expression data using real-time quantitative PCR and the 2(-Delta Delta C(T)) Method. Methods *25*, 402–408.

Maione, T.E., Gray, G.S., Petro, J., Hunt, A.J., Donner, A.L., Bauer, S.I., Carson, H.F., and Sharpe, R.J. (1990). Inhibition of angiogenesis by recombinant human platelet factor-4 and related peptides. Science *247*, 77–79.

Mantovani, A., Allavena, P., Sica, A., and Balkwill, F. (2008). Cancer-related inflammation. Nature *454*, 436–444.

Mantovani, A., Sica, A., and Locati, M. (2005). Macrophage polarization comes of age. Immunity *23*, 344–346.

Mazzieri, R., Pucci, F., Moi, D., Zonari, E., Ranghetti, A., Berti, A., Politi, L.S., Gentner, B., Brown, J.L., Naldini, L., and De Palma, M. (2011). Targeting the ANG2/TIE2 axis inhibits tumor growth and metastasis by impairing angiogenesis and disabling rebounds of proangiogenic myeloid cells. Cancer Cell *19*, 512–526.

Mitchem, J.B., Brennan, D.J., Knolhoff, B.L., Belt, B.A., Zhu, Y., Sanford, D.E., Belaygorod, L., Carpenter, D., Collins, L., Piwnica-Worms, D., et al. (2013). Targeting tumor-infiltrating macrophages decreases tumor-initiating cells, relieves immunosuppression, and improves chemotherapeutic responses. Cancer Res. *73*, 1128–1141.

Motz, G.T., and Coukos, G. (2011). The parallel lives of angiogenesis and immunosuppression: cancer and other tales. Nat. Rev. Immunol. *11*, 702–711.

Motz, G.T., and Coukos, G. (2013). Deciphering and reversing tumor immune suppression. Immunity *39*, 61–73.

Pahler, J.C., Tazzyman, S., Erez, N., Chen, Y.Y., Murdoch, C., Nozawa, H., Lewis, C.E., and Hanahan, D. (2008). Plasticity in tumor-promoting inflammation: impairment of macrophage recruitment evokes a compensatory neutrophil response. Neoplasia *10*, 329–340.

Pucci, F., Venneri, M.A., Biziato, D., Nonis, A., Moi, D., Sica, A., Di Serio, C., Naldini, L., and De Palma, M. (2009). A distinguishing gene signature shared by tumor-infiltrating Tie2-expressing monocytes, blood "resident" monocytes, and embryonic macrophages suggests common functions and developmental relationships. Blood *114*, 901–914.

Qian, B.Z., and Pollard, J.W. (2010). Macrophage diversity enhances tumor progression and metastasis. Cell *141*, 39–51.

Rigamonti, N., Kadioglu, E., Keklikoglou, I., Wyser Rmili, C., Leow, C.C., and De Palma, M. (2014). Role of angiopoietin-2 in adaptive tumor resistance to VEGF signaling blockade. Cell Rep. *8*, 696–706.

Rommel, C., Camps, M., and Ji, H. (2007). PI3K delta and PI3K gamma: partners in crime in inflammation in rheumatoid arthritis and beyond? Nat. Rev. Immunol. *7*, 191–201.

Ryder, M., Gild, M., Hohl, T.M., Pamer, E., Knauf, J., Ghossein, R., Joyce, J.A., and Fagin, J.A. (2013). Genetic and pharmacological targeting of CSF-1/CSF-1R inhibits tumor-associated macrophages and impairs BRAF-induced thyroid cancer progression. PLoS ONE *8*, e54302.

Schaerli, P., Willimann, K., Ebert, L.M., Walz, A., and Moser, B. (2005). Cutaneous CXCL14 targets blood precursors to epidermal niches for Langerhans cell differentiation. Immunity *23*, 331–342.

Schmid, M.C., Avraamides, C.J., Dippold, H.C., Franco, I., Foubert, P., Ellies, L.G., Acevedo, L.M., Manglicmot, J.R., Song, X., Wrasidlo, W., et al. (2011). Receptor tyrosine kinases and TLR/IL1Rs unexpectedly activate myeloid cell PI3kg, a single convergent point promoting tumor inflammation and progression. Cancer Cell *19*, 715–727.

Schoenfeld, J.D., and Dranoff, G. (2011). Anti-angiogenesis immunotherapy. Hum. Vaccin. *7*, 976–981.

Sharpe, R.J., Byers, H.R., Scott, C.F., Bauer, S.I., and Maione, T.E. (1990). Growth inhibition of murine melanoma and human colon carcinoma by recombinant human platelet factor 4. J. Natl. Cancer Inst. *82*, 848–853.

Shellenberger, T.D., Wang, M., Gujrati, M., Jayakumar, A., Strieter, R.M., Burdick, M.D., Ioannides, C.G., Efferson, C.L., El-Naggar, A.K., Roberts, D., et al. (2004). BRAK/CXCL14 is a potent inhibitor of angiogenesis and a chemotactic factor for immature dendritic cells. Cancer Res. *64*, 8262–8270.

Shojaei, F., Wu, X., Malik, A.K., Zhong, C., Baldwin, M.E., Schanz, S., Fuh, G., Gerber, H.P., and Ferrara, N. (2007a). Tumor refractoriness to anti-VEGF treatment is mediated by CD11b+Gr1+ myeloid cells. Nat. Biotechnol. *25*, 911–920.

Shojaei, F., Wu, X., Zhong, C., Yu, L., Liang, X.H., Yao, J., Blanchard, D., Bais, C., Peale, F.V., van Bruggen, N., et al. (2007b). Bv8 regulates myeloid-cell-dependent tumour angiogenesis. Nature *450*, 825–831.

Squadrito, M.L., Pucci, F., Magri, L., Moi, D., Gilfillan, G.D., Ranghetti, A., Casazza, A., Mazzone, M., Lyle, R., Naldini, L., and De Palma, M. (2012). miR-511-3p modulates genetic programs of tumor-associated macrophages. Cell Rep. *1*, 141–154.

Talmadge, J.E., and Gabrilovich, D.I. (2013). History of myeloid-derived suppressor cells. Nat. Rev. Cancer *13*, 739–752.

Wynn, T.A., Chawla, A., and Pollard, J.W. (2013). Macrophage biology in development, homeostasis and disease. Nature *496*, 445–455.

Yang, L., Huang, J., Ren, X., Gorska, A.E., Chytil, A., Aakre, M., Carbone, D.P., Matrisian, L.M., Richmond, A., Lin, P.C., and Moses, H.L. (2008). Abrogation of TGF beta signaling in mammary carcinomas recruits Gr-1+CD11b+ myeloid cells that promote metastasis. Cancer Cell *13*, 23–35.